UCRL-LR-103225
Distribution Category UC-405

The POWER Codes for Estimating Reflected Light into an Off-Axis Optical Fiber

D. R. Goosman

Manuscript date: March 2, 1991

LAWRENCE LIVERMORE NATIONAL LABORATORY
University of California • Livermore, California • 94551

Available to DOE and DOE contractors from the Office of Scientific and Technical Information
P.O. Box 62, Oak Ridge, TN 37831 Prices available from (615) 576-8601, FTS 626-8401

Available from: National Technical Information Service • U.S. Department of Commerce
5285 Port Royal Road • Springfield, VA 22161 • A03 • (Microfiche A01)

Contents

Abstract 1
Introduction 1
Ray Tracing from the Laser Fiber 2
Ray Tracing from the Reflector to the Fiber Plane 4
Calculating Light vs Radius 5
Calculating Reflected Light Entering 7
Inputs for the POWER Code 10
POWERE, the Next Better Code 10
POWERX, a Better Code 12
POWERX8—the Most Accurate Code 13
Summary 17
References 17
Appendix: Format of the POWER Code 18

The POWER Codes for Estimating Reflected Light into an Off-Axis Optical Fiber

Abstract

We give a calculation for estimating the amount of laser light collected by an off-axis optical fiber for velocimetry applications. It is assumed that laser light emanating from a single optical fiber is transported to a Lambertian reflector by a two-element lens composed of three spherical surfaces; an off-axis optical fiber adjacent to the laser fiber collects the light used for velocimetry. Four Symphony spreadsheets—POWER, POWERE, POWERX, and POWERX8—are available to trace rays from the laser fiber through the compound lens onto the Lambertian surface to calculate the blur due to spherical aberration and to being out of focus. POWER uses the most approximations and is the fastest, while POWERX8 is the most accurate and slowest.

POWER assumes that the light distribution on the Lambertian reflector due to a point source within the laser fiber is flat out to either a maximum radius or an effective radius determined by the ray-tracing routine. This flat distribution is then convolved in two dimensions with the round shape of the laser fiber to provide an analytic formula for light incident on the reflecting surface vs radius. Tracing rays in reverse through the lens provides the size of the illumination at the fiber plane containing all of the light due to a point source at the reflector, as well as a smaller effective size. The radial distribution within this circle is assumed to be flat. The result is convolved with the radial distribution on the reflector to estimate how much light enters the collection fiber as a function of the position of the reflector.

POWERE calculates the actual radial distribution of light on the reflector due to a point source at the laser fiber in ten radial bins. However, the distribution at the fiber plane due to a point source at the reflector is still assumed to be flat, as in the POWER code.

POWERX relaxes the assumption for POWERE by using ten radial bins at the fiber plane.

POWERX8 is the same as POWERX, except that there are 20, rather than 10, bins at both the reflector and the fiber plane, and a fiber-plane illumination distribution is also calculated.

Introduction

Laser velocimetry has been used at Lawrence Livermore National Laboratory (LLNL) and elsewhere for many years to provide detailed velocity-time data for rapidly moving surfaces.[1] We originally used a single-field lens to transport a laser beam to and from a test surface, because that method is very light-efficient if the distance between the velocimeter and the surface is not too great. As that distance increases, however, vignetting losses become great unless a complicated optical train is used in place of a single field lens. Under these conditions, fiber-optic transport becomes as efficient as air transport via a single field lens, and the fiber

technique is easier to use. Fiber-optic transport has a disadvantage relative to air transport in that the brightness of the beam (power per unit area per unit solid angle) is usually degraded. Degradation can occur if either the spatial size or the numerical aperture of the fibers is underfilled.

We plan to use the new striped interferometers[2,3] because they transmit more light than conventional ones, even when finite surface travel is included. Under these conditions, it appears from calculations that little power gain can be realized from using more than one collection fiber. In addition, multiple collection fibers would increase complexity. Accordingly, we consider here only two fibers, one to bring the laser light to the field lens and one to collect some of the Doppler-shifted light.

Figure 1 shows our optical configuration. The compound lens is azimuthally symmetric, and the index of refraction of either piece may be set equal to unity to simulate a single lens. One problem with this geometry is that the collection fiber and laser fiber cannot be on the same axis if they are located in the same plane. If the reflector were in perfect focus (for an aberration-free lens), all the collection light would miss the collector fiber! Consequently, the curve of collection light vs reflector position would dip severely as the reflector moved through focus. Real lens aberrations fill in the dip somewhat, however.

The present codes allow the collection fiber to be off axis by any amount, including zero. Thus, simulations of the geometry shown in Fig. 1 can be estimated, but one can also put the collection fiber on axis.

Ray Tracing from the Laser Fiber to the Reflector

We first consider only the light emanating from a point on axis within the laser fiber. Figure 2 defines the parameters. The origin of coordinates is defined as a distance $T/2$ to the right of the leftmost surface of the compound lens; that is, at the middle of the biconvex part. A ray leaving the laser fiber on axis at point n and angle δ' traverses the lens and crosses the axis at point a with angle θ. Since point n is on the axis, only meridional rays need be traced. From the triangle n-g-m, we have

$$x_n = x_g + \frac{r_3' \cdot \sin\phi_5}{\sin\delta'} \tag{1}$$

and

$$\phi_5 = \sin^{-1}\left[\frac{(x_n - x_g)\sin\delta'}{r_3'}\right]. \tag{2}$$

Snell's law implies that

$$\phi_4 = \sin^{-1}\left(\frac{\sin\phi_5}{n_2'}\right). \tag{3}$$

The relations

$$\tan\delta' = \frac{y_m}{x_n - x_m} \equiv \frac{y_m}{x_{nm}} \tag{4}$$

and

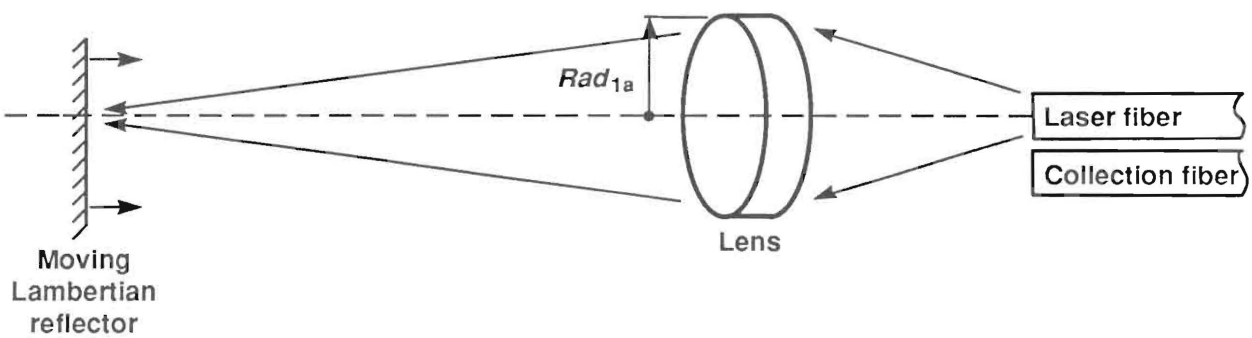

Figure 1. An optical fiber illuminates a two-element lens of radial aperture Rad_{1a}, which transports the light to a moving Lambertian reflector. Some of the reflected light is collected by the lens and is transported into the collection fiber, which may be either off or on axis in the code.

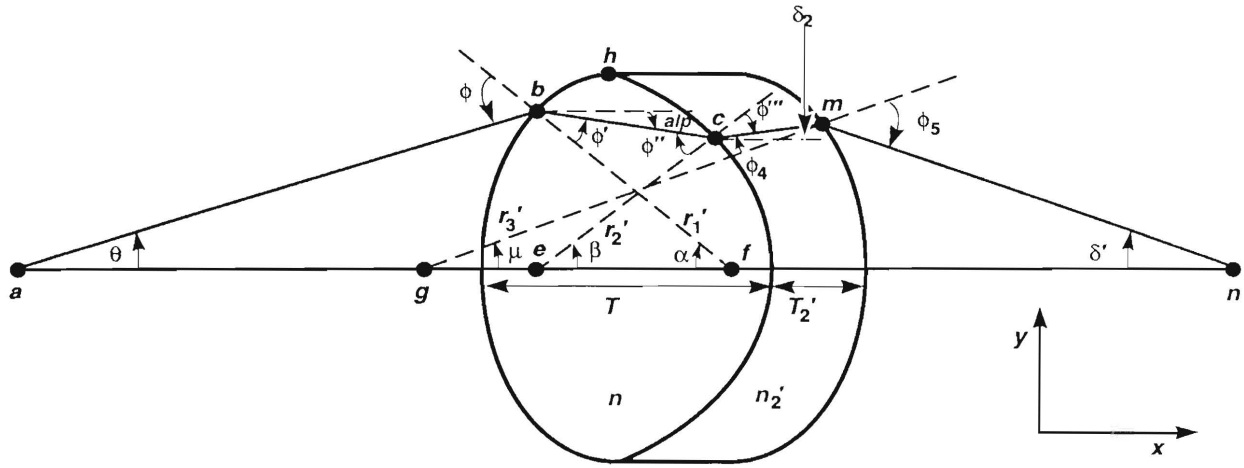

Figure 2. The ray-tracing geometry being considered. Light from an on-axis point of the laser fiber at point *n* crosses the axis at point *a* on the reflector side of the lens. All radii and angles shown are positive. The left section of the lens of thickness *T* has index of refraction *n*. The right section has thickness T_2' and index n_2'. See the Appendix for definitions of r_1', r_2', and r_3'.

$$y_m^2 + x_{mg}^2 = (r_3')^2 \tag{5}$$

allow determination of the intersection point *m*. We define

$$x_{mg} \equiv x_m - x_g \ . \tag{6}$$

Equations (4) through (6) then imply that

$$x_{mn}^2 (1 + \tan^2\delta') + x_{mn} (2x_{ng}) + x_{ng}^2 - (r_3')^2 = 0 \ , \tag{7}$$

from which we obtain x_m by using the positive solution and y_m from Eq. (5).

From Fig. 2, we see that

$$\mu = \sin^{-1} \frac{y_m}{r_3'} \tag{8}$$

and

$$\delta_2 = \mu - \phi_4 \tag{9}$$

and

$$x_{ce}^2 + y_c^2 = (r_2')^2 \ . \tag{10}$$

Figure 2 implies that

$$y_{mc} = \tan\delta_2 \cdot x_{mc} \ , \tag{11}$$

from which one can construct the quadratic relation

$$x_{cm}^2 (1 + \tan^2\delta_2) + x_{cm} (2x_{me} + 2y_m \cdot \tan\delta_2) + x_{me}^2 + y_m^2 - (r_2')^2 = 0 \ . \tag{12}$$

Equation (12) determines the *x* coordinate of the intersection point *c*, and its *y* coordinate is obtained from Eq. (11):

$$y_c = y_m - y_{mc} \ . \tag{13}$$

From Fig. 2 we then see that

$$\beta = \sin^{-1} \frac{y_c}{r_2'} \tag{14}$$

and

$$\phi''' = \beta - \delta_2 \ , \tag{15}$$

so that

$$\phi'' = \sin^{-1} \left(\frac{n_2' \cdot \sin\phi'''}{n} \right) \tag{16}$$

and

$$alp = \phi'' - \beta \ . \tag{17}$$

To find x_b, we see from Fig. 2 that

$$x_{fb}^2 + y_b^2 = (r_1')^2 \tag{18}$$

and

$$y_{bc} = x_{cb} \cdot \tan alp \ , \tag{19}$$

which can be combined to give the quadratic in x_{bc},

$$x_{bc}^2 (1 + \tan^2 alp) + x_{bc} (2x_{cf} - 2y_c \cdot \tan alp) + x_{cf}^2 + y_c^2 - (r_1')^2 = 0 \ . \tag{20}$$

Then, from Eq. (19),

$$y_b = y_c - x_{bc} \cdot \tan alp \ . \tag{21}$$

Since

$$\alpha = \sin^{-1} \frac{y_b}{r_1'} \ , \tag{22}$$

$$\phi' = \alpha - alp \ , \tag{23}$$

and

$$\phi = \sin^{-1} (n \cdot \sin \phi') \ , \tag{24}$$

we can use the relation

$$\theta = \phi - \alpha \tag{25}$$

to finally determine the x coordinate of the crossing point a as

$$x_{fa} = \frac{r_1' \cdot \sin\phi}{\sin\theta} \ . \tag{26}$$

The y coordinate of this final ray crossing an arbitrary plane whose x coordinate = x_{plane} is then

$$\text{offset} = \left| (x_{plane} - x_a) \tan\theta \right| \ . \tag{27}$$

This gives the radial offset distance of the ray that intercepts the moving reflector. By running a set of rays of increasing δ', one can determine the maximum size and radial distribution of light within the blur spot on the reflector due to an on-axis point source from the laser fiber. In the POWER code, we approximate this distribution by a distribution that is assumed flat out to radius r_t, which can be either the maximum radial offset of the set of rays or a smaller value determined by weighting each offset value by the number of rays launched with the corresponding value of δ'.

The error introduced by assuming a flat blur distribution is probably greatest when the reflector is closest to the circle of least confusion, or "in focus." As the reflector moves away from this point, the blur is dominated not by spherical aberration but by being out of focus. Here the distribution tends to be flat. The ray-tracing routine that calculates the radial offsets includes both aberration and the out-of-focus effects together. Monte Carlo programs could include the exact blur distribution, but the assumption of flatness allows the calculation to proceed without any further approximations by a very rapid and convenient personal computer (PC) spreadsheet method.

We assume that the diameter of the laser fiber is very small compared with the diameter of the lens, and the blur distribution on the reflector due to an off-axis point within the laser fiber is therefore nearly identical to that due to an on-axis point. This is because the difference between ray angles for the off- and on-axis source points is very small. Thus, coma distortion is neglected.

Ray Tracing from the Reflector to the Fiber Plane

By using formulas similar to those given above, the codes run a set of rays of different θ values from an on-axis point on the reflector to the plane of the collection fiber. The result is a blur distribution named r_t', which, in the POWER code, can represent either the maximum size of the blur or a weighted value. In POWER, the distribution is assumed to be flat, and coma is neglected. POWER also increases, by a term, the value of the blur determined by ray-tracing to allow for diffraction, although the latter is almost always negligible.

Calculating Light vs Radius on the Reflector

Figure 3 shows light from a single off-axis point on the laser fiber illuminating a circular region of radius rt on the reflector. The center of this illumination is at a radius

$$r_{1o} = r_1 \cdot \left(\frac{S_{1a} + H_{left}}{L_{1f} - H_{right}}\right) . \tag{28}$$

We now add at the reflector the contributions from all the possible source points of the laser fiber. Figures 4(a) to 4(c) illustrate the three possibilities for the total light at radius r on the reflector. In each of these figures, the shaded overlap region represents the position of all possible r_{1o} positions (illumination centers from unique points at the laser fiber) that lie with a distance r_t of the test point on the reflector at radius r. Here we have defined

$$r_0 = R_{1fib}\left(\frac{S_{1a} + H_{left}}{L_{1f} - H_{right}}\right) . \tag{29}$$

In Fig. 4(a), r_t may be smaller or larger than r_0, but the two circular boundaries intersect at a distance x_1' from the axis along the line joining their two centers. It is easy to show that

$$x_1' = r - \eta_t \cdot r_t = \frac{r^2 + r_0^2 - r_t^2}{2r} , \tag{30}$$

where η_t is defined by

$$\eta_t = \frac{r - x_1'}{rt} . \tag{31}$$

Let P denote the watts of light emitted by the entire laser fiber that is intercepted by the lens. Then, a very small area of that fiber, dA_f, emits $P \cdot dA_f / A_f$ watts, which illuminate an area πr_t^2 at the reflector. The power per unit area on the reflector due to this one area dA_f is

$$\frac{P \cdot dA_f}{A_f \cdot \pi \cdot r_t^2} . \tag{32}$$

The number of separate surface elements dA_t on the fiber that contribute to the light on the reflector at radius r is just

$$\frac{F \cdot \pi \cdot R_{1fib}^2}{dA_f} , \tag{33}$$

where F is the fractional area of the fiber that has r_{1o} points within a distance r_t of the point r, as shown in Fig. 4(a). Since F can be written

$$F = \frac{\text{shaded area}}{\pi \cdot r_0^2} , \tag{34}$$

we can combine Eqs. (32) through (34) to deduce the power per unit area on the reflector as a function of radius:

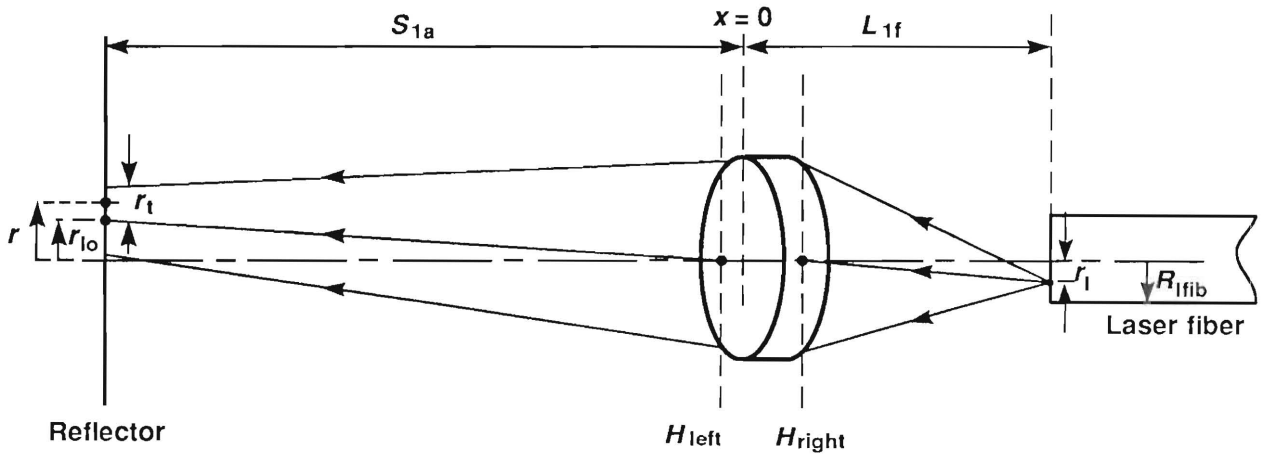

Figure 3. Light from a single point on the laser fiber illuminates a spot of radius r_t (determined by ray tracing) at the reflector. The left and right principal points H are shown. S_{1a} and L_{1f} are measured to the origin of coordinates, which is midway between the two leftmost surfaces of the lens.

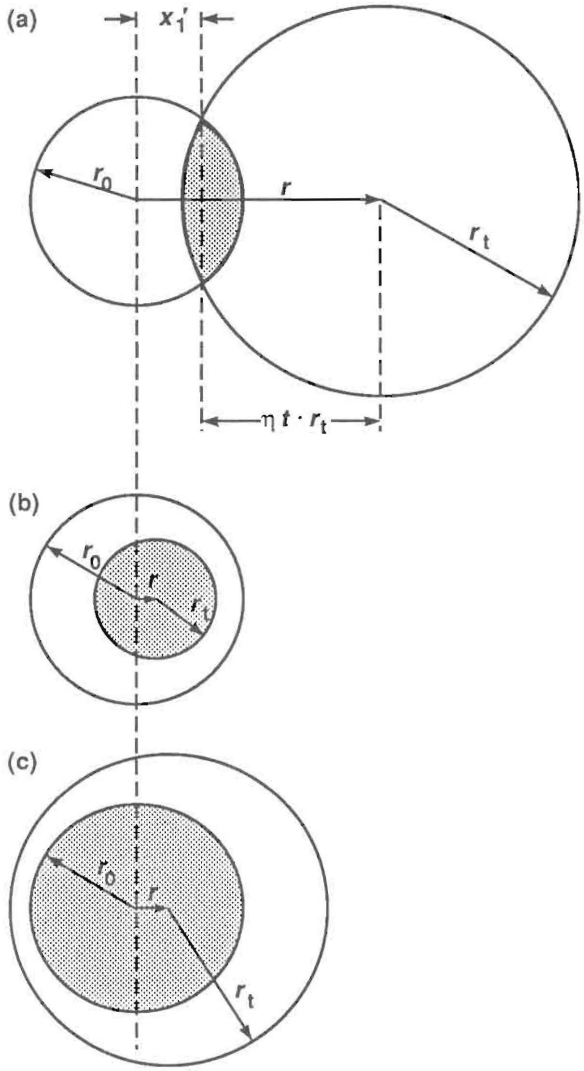

Figure 4. Three possibilities for the overlap at the reflector of the blur circle of radius r_t and the circle of radius r_0, which contains the centers of illumination due to all source points from the laser fiber. These figures are used in calculating the intensity at radius r on the reflector.

$$I_r(r) = \frac{\text{shaded area}}{\pi \cdot r_0^2} \left(\frac{\pi \cdot R_{\text{lfib}}^2}{dA_f}\right)\left(\frac{P}{A_f}\,\frac{dA_f}{\pi \cdot r_t^2}\right)$$

$$= \frac{P \cdot \text{shaded area}}{\pi \cdot r_0^2 \cdot \pi \cdot r_t^2} . \qquad (35)$$

The overlap area in Fig. 4(a) can be determined by noting from Fig. 5 that the fractional shaded area is given by

$$\frac{\text{shaded}}{\text{total}} = \frac{1}{2} - \frac{\eta\sqrt{1-\eta^2}}{\pi} - \frac{\sin^{-1}\eta}{\pi} \equiv g(\eta) . \qquad (36)$$

Then the overlap area in Fig. 4(a) is obtained as the sum of a fraction of the area of the r_0 circle and another fraction of the area of the r_t circle.

The two cases illustrated by Figs. 4(b) and 4(c) have an overlap area equal to the area of the smaller of the two circles. Thus, all three cases can be combined into the following relations for the power per unit area on the reflector:

$$I_r = \frac{P}{\pi\,[\max(r_0, r_t)]^2} \qquad (37)$$

if $0 \le r \le |\, r_0 - r_t \,|$

and

$$Ir = \frac{P}{\pi \cdot r_t^2}\, g(\eta_0) + \frac{P}{\pi \cdot r_0^2}\, g(\eta_t) \qquad (38)$$

if $|\, r_0 - r_t \,| < r \le |\, r_0 + r_t \,|$, where we have defined

$$\eta_0 = \frac{x_1'}{r_0} , \qquad (39)$$

and ηt and x_1' were defined by Eqs. (30) and (31), respectively.

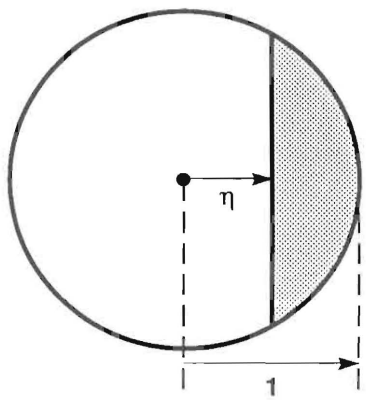

Figure 5. The shaded area divided by the total circular area is given by Eq. (36).

The above result shows that unless r_0 and r_t are equal, the illumination on the reflector will be flat from $r = 0$ out to a finite radius. It then drops off smoothly and becomes zero at $r = r_0 + r_t$. One must keep in mind, however, that these results assume a flat blur function (from ray tracing) due to light from a single point on the laser fiber. The ray-tracing routine also assumes that light from a single point on the laser fiber has an angular distribution that is flat out to some angle and then is zero for larger angles. If the cutoff angle occurs within the lens, then the routine limits the angle of the rays to stay within that cutoff.

Calculating Reflected Light Entering the Collection Fiber

Figure 6 shows a collection fiber off axis by an amount S_f that may be zero. Each small area dA_r on the reflector at radius r has an illumination energy $I_r \cdot dA_r$. The fraction intercepting the lens that can make exit rays within the numerical aperture of the collection fiber is approximately

$$F\Omega = \left\{ \frac{\min[Rad_{1a}, (L_{1f} - T/2 - T_2')\tan(\sin^{-1} NA_c)]}{S_{1a}} \right\}^2 \tag{40}$$

for a perfectly reflecting Lambertian surface.

The energy per unit area at the fiber plane due to this single spot on the reflector is

$$dI_c = \frac{I_r \cdot dA_r \cdot F\Omega}{\pi \cdot (r_t')^2} \ . \tag{41}$$

This energy is distributed over a circle of radius r_t' (determined by the second ray-tracing part) whose center is at a radius r_0'. Figures 7(a) through 7(c) show, for the three possible cases, how this illumination overlaps an off-axis collection fiber of radius R_{cfib}. The energy entering the fiber from this one spot on the reflector is dI_c times the overlap area of Fig. 7(a). The integration over all contributions from spots on the reflector is complicated by the fact that the collection fiber is off axis in general. To do the calculation, we need to know the distance w as a function of r_0' and ϕ. The result is

$$w = \sqrt{(r_0')^2 - 2r_0' \cdot S_f \cdot \cos\phi + S_f^2} \ . \tag{42}$$

Then we can determine the overlap area by defining

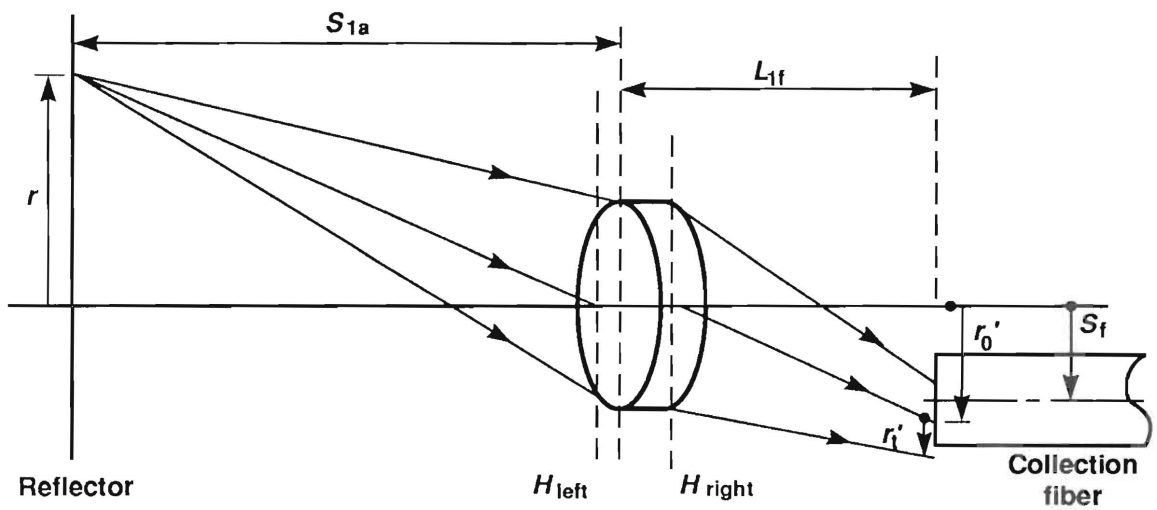

Figure 6. A point source at radius r on the reflector makes a circle of illumination at the fiber plane of radius r_t'. This is partially intercepted by a collection fiber of offset S_f (which may be zero).

$$x_1'' = \frac{w^2 + R_{\text{cfib}}^2 - (r_t')^2}{2 \cdot w} \ , \tag{43}$$

$$\eta_0' = \frac{x_1''}{R_{\text{cfib}}} \ , \tag{44}$$

and

$$\eta_t' = \frac{w - x_1''}{r_t'} \ . \tag{45}$$

The overlap areas for Figs. 7(a) to 7(c) are

$$\text{overlap} = \pi \cdot \min\left[R_{\text{cfib}}^2, (r_t')^2\right] \tag{46}$$

if $0 \le w \le \left| R_{\text{cfib}} - r_t' \right|$, and

$$\text{overlap} = \pi \cdot (rt')^2 \cdot g(\eta_t') + \pi \cdot R_{\text{cfib}}^2 \cdot g(\eta_0') \tag{47}$$

if $\left| R_{\text{cfib}} - r_t' \right| < w < r_t' + R_{\text{cfib}}$.

To do the integration over all source spots on the reflector for the case of Fig. 7(a), we let r vary from zero to $r_0 + r_t$. If $S_f = 0$, the maximum value of ϕ is π; otherwise, it is less. Figure 8 is drawn for the largest value of ϕ that can make overlap, since r_0', R_{cfib}, and r_t' are fixed. For an off-axis collection fiber, S_f is not equal to zero, and $\phi_{\max}$ is just

$$\phi_{\max} = \min\left\{\pi, \cos^{-1}\left[\frac{(r_0')^2 + S_f^2 - (r_t' + R_{\text{cfib}})^2}{2 \cdot r_0' \cdot S_f}\right]\right\} . \tag{48}$$

Thus, the range of ϕ values in the integration changes as the radial position of the source spot on the reflector increases.

Figure 9 shows that the minimum value of r_0' to be considered is

$$r_{0\,\min}' = \max\left(S_f - R_{\text{cfib}} - r_t', 0\right) \ . \tag{49}$$

The maximum value of r_0' needed is, from Fig. 10,

$$r_{0\,\max}' = \min\left[S_f + R_{\text{cfib}} + r_t', \ (r_0 + r_t)\,\frac{L_{1f} - H_{\text{right}}}{S_{1a} + H_{\text{left}}}\right] , \tag{50}$$

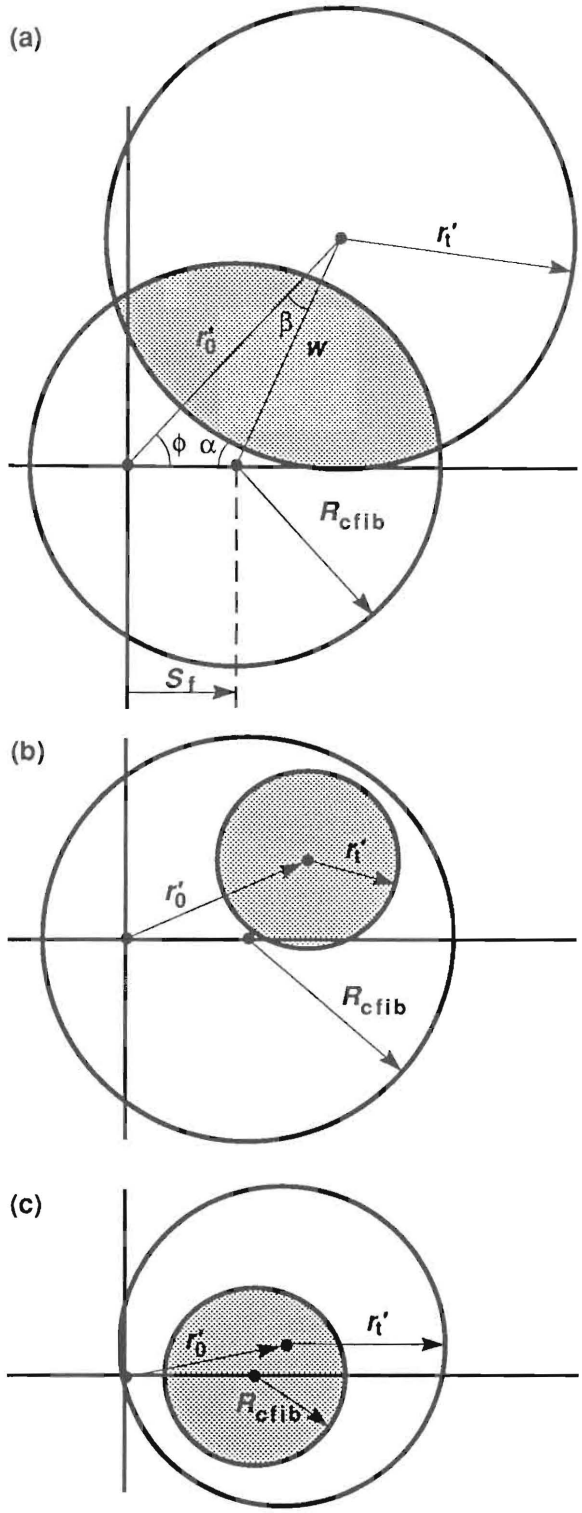

Figure 7. Three possibilities for the overlap at the fiber plane of the blur circle of radius r_t' and the collection fiber, for a fixed value of r_0' at the fiber plane (or a fixed value of r at the reflector).

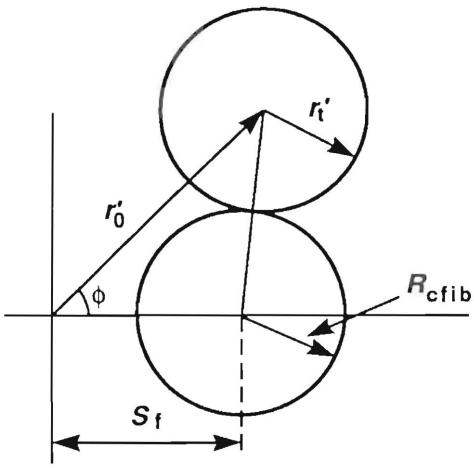

Figure 8. A special case of Fig. 7 from which ϕ max is determined, given that r_0', r_t', R_{cfib}, and S_f are fixed.

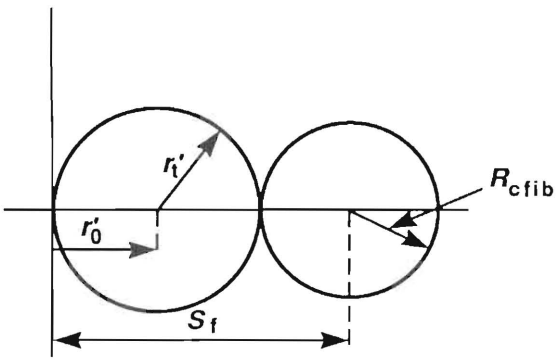

Figure 9. A special case of Fig. 7 from which the minimum value of r_0' is determined.

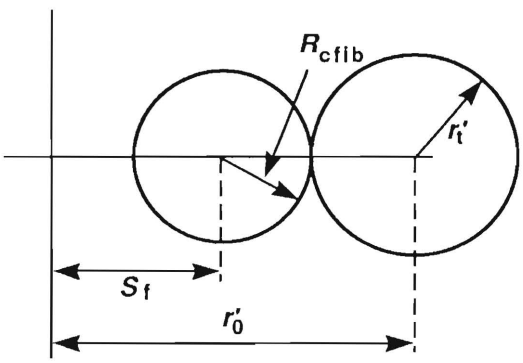

Figure 10. A special case of Fig. 7 from which the maximum value of r_0' is determined.

where the second term arises from the fact that illumination at the reflector (see Fig. 3) does not exist for r larger than $r_0 + r_t$. Thus, the center of illumination r_0' at the fiber plane (see Fig. 6) cannot exceed $(L_{1f} - H_{right})/(S_{1a} + H_{left}$ times that limit, where H_{right} and H_{left} are the positions of the right and left principal points of the lens.

At the reflector plane (see Fig. 11), the energy entering the collection fiber from an annulus of thickness dr and width $d\phi$ is

$$I_\phi = \frac{d\phi \cdot I_r \cdot rdr \cdot F\Omega \cdot \text{overlap}}{\pi (r_t')^2} \quad . \tag{51}$$

In the POWER code, values for Eq. (51) are summed over ten values of ϕ for a given value of r_0' to give the quantity called I_{cr}, and then summed over r_0' to give the quantity called "power" in the code. This double summation is done by filling a two-dimensional area of the spreadsheet and using the "calculate" command, rather than by using macros because the latter would increase computation time significantly.

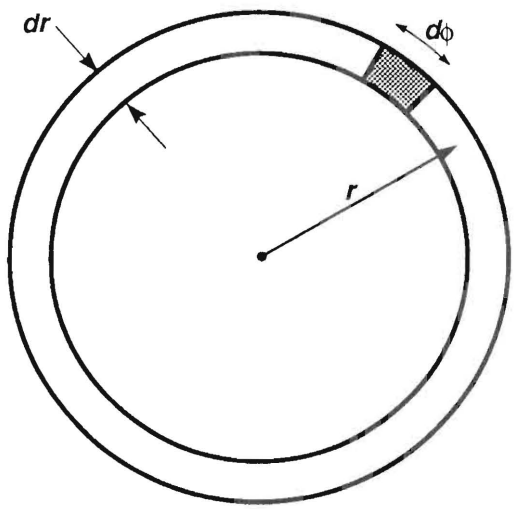

Figure 11. Radial and angular integration elements at the reflector plane.

Inputs for the POWER Code

The Appendix explains the inputs of the POWER code. Figure 12 and Figure A-1 show a curve of collected light vs reflector position calculated with POWER. For comparison, results of a Monte-Carlo code written by C. McMillan[4] are also shown. The deviation between the two curves should be treated as being the result of the approximations in the POWER code.

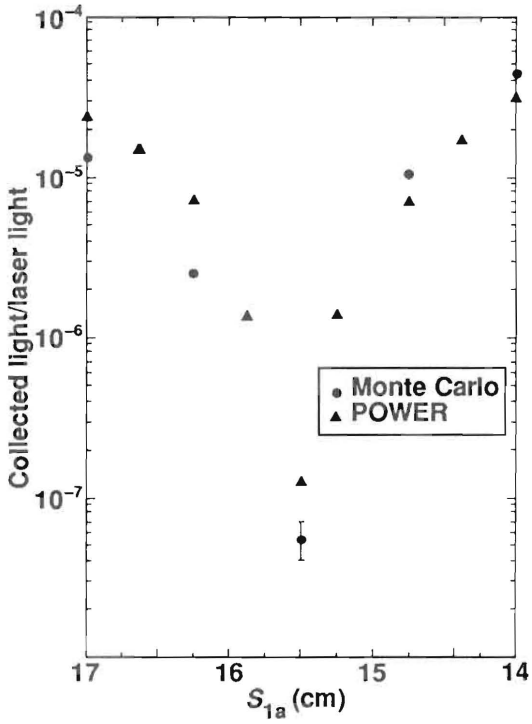

Figure 12. The collected light vs reflector travel position as estimated by POWER and McMillan's Monte Carlo calculation.

POWERE, the Next Better Code

Although POWER is fast (about 25 s for nine reflector positions), its accuracy is limited. Thus, the code POWERE was written, which is slower but calculates the radial dependence of the power distribution on the reflector from a point source at the laser fiber much better than POWER does.

A point source on the laser fiber makes a uniformly illuminated circular illumination at the reflector in the POWER code, whose diameter is the smallest circle containing all of the light, or a smaller value, weighted by the numbers of rays launched. In POWERE, the fan of ten ray angles δ' launched from an on-axis point at the laser fiber to the reflector intercepts the reflector at ten different radii r_{ti} . These intercept radii do not necessarily increase monotonically with the launch angle δ'. For many situations, as δ' increases from zero to its maximum value, r_{ti} first increases from zero, reaches a maximum, and then decreases.

This not-flat radial distribution of illumination is incorporated into the POWERE code in a fairly simple way. Rays with angle δ' are launched in ten angular bins, making ten annular bins at the reflector. Each of the ten annular bins has a value of r_{tmin} and r_{tmax}, and a known fraction F_r of the rays launched. In Fig. 4 for POWER, a uniformly illuminated circle of radius r_t was convolved (analytically) with a source fiber of radius r_0 (referred to the target), producing the simple result of Eqs. (37) through (39). In POWERE, we convolve each annular bin by treating it as the difference between two circu lar bins of radius r_{tmax} and r_{tmin}, respectively. The weight of each of these two circular bins is adjusted to match the weight per unit area of the original annular bin.

Figure 13 shows the decomposition of the annular bin into the two circular bins. The fractions F_{r1} and F_{r2} of rays needed in the two bins are given by

$$\frac{F_{r1}}{r_{tmax}^2} = \frac{F_{r2}}{r_{tmin}^2} = \frac{F_r}{r_{tmax}^2 - r_{tmin}^2} \ . \qquad (52)$$

The same routine used in POWER to convolve the two circles together is used twice in

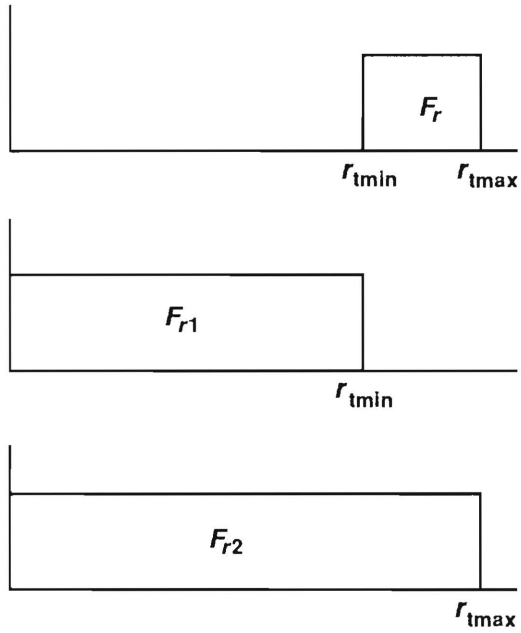

Figure 13. The decomposition of the annular illumination at the reflector into two circles.

POWERE to convolve the required annulus with the laser fiber size.

The quantity I_r of Eqs. (37) through (39) is evaluated in POWERE for r_{tmax} and for r_{tmin}. Then the power per unit area at the reflector due to the one annular bin is

$$I_{rsetnet} = \frac{F_r}{r_{tmax}^2 - r_{tmin}^2} \cdot [I_r(r_{tmax}) \cdot r_{tmax}^2 - I_r\ (r_{tmin}) \cdot r_{tmin}^2] \ . \qquad (53)$$

$I_{rsetnet}$ is calculated for each of the ten annular bins and summed to give the proper value for I_r for Eq. (51), which is still used to determine the collected light in POWERE. As in POWER, the illumination at the reflector, I_r is calculated only for values of r that could possibly contribute to the light entering the collection fiber.

User input to POWERE is slightly different than for POWER. Figure A-2 shows the input/output area of POWERE. In the latter, using "maximum blurs" in the appropriate cell will affect only the r_t' distribution at the fiber plane, since the r_t distribution at the reflector is automatically binned. Also, instead of R_{lower} and R_{upper}, POWERE uses $R(I_{max})$ and $R(I = 0)$, which are the radii at the reflector for maximum and zero intensity, respectively.

Figure 14 shows the POWERE prediction vs McMillan's Monte Carlo calculation for the same situation as illustrated in Fig. 12 for POWER. The agreement is better. Figure 14 also shows the radius R_{half} at which the illumination on the reflector is half its maximum value as calculated by POWERE and the Monte Carlo code. It is important for certain experiments with velocimetry to keep the value of R_{half} small. A special version of POWERE was written using 20 blur bins rather than 10, but no significant improvement in accuracy resulted. Like POWER, POWERE uses ten ϕ and ten radial bins in calculating what fraction of the fiber-plane illumination enters the collection fiber. Nine reflector positions are calculated in about 60 s. A simple macro is used to vary S_{1a}, but the rest of the calculations are done without macros to minimize computation time.

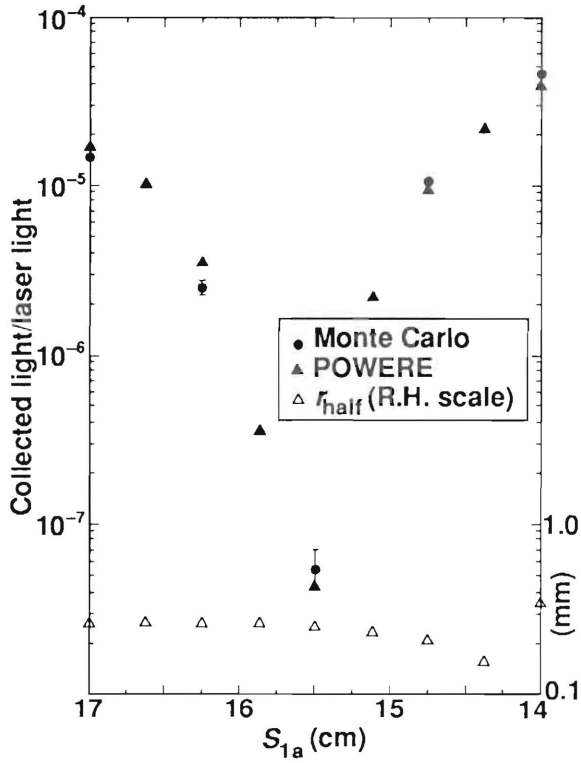

Figure 14. Collected light vs reflector travel position as estimated by POWERE and the Monte Carlo calculations (L.H. scale). The largest radius at which the illumination on the reflector is half its maximum value vs reflector position, as determined by POWERE and Monte Carlo (R.H. scale).

Finally, the assumption of a flat distribution of light at the fiber plane due to a fixed point on the reflector is relaxed. In POWERX, light from an on-axis reflector source point is put into ten annular r_t' bins (determined by ray tracing) at the fiber plane. We assume that coma is negligible. Thus the binned r_t' blur distribution at the fiber plane due to an off-axis point at the reflector has the same shape as that due to an on-axis point, but is shifted in position.

POWERX uses the formalism of the preceding codes to first calculate how much reflected light in a specific r_t' bin summed over all contributing positions at the reflector enters the collection fiber. It then sums over the ten r_t' bins to determine the total light collected.

Figure 15 shows the annular illumination at the fiber plane due to light leaving an small area $r \cdot dr \cdot d\phi$ of the reflector (see Fig. 11) due to just one of the ten r_t' bins. The annulus has outer and inner radii $r_t'_{up}$ and $r_t'_{low}$, respectively. The shaded area in Fig. 15 is calculated to determine how much of that annulus of light enters the collection fiber. Figure 15 is analogous to Fig. 4 for the POWER code, except we have an annulus rather than a circle.

In POWERX, the shaded area is calculated by taking the difference between the overlap of the $r_t'_{up}$ and $r_t'_{low}$ circles. POWERX evaluates the overlap of the $r_t'_{up}$ and $r_t'_{low}$ circles by using the formalism of the preceding codes. For a given r_t' bin, a range of r_0' values is determined by equations analogous to Eqs. (49) and (50), except that r_t' there is replaced by $r_t'_{up}$ or $r_t'_{low}$, depending on which circular overlap is being calculated. This range of r_0' values determines a range of r values at the reflector by multiplying by the magnification.

For each r_t' bin, the relevant area on the reflector that can contribute is divided up into ten radial bins times ten ϕ bins. This binning is done efficiently in order to not waste bins on areas than cannot contribute. The light from the 100 combinations of radial and ϕ bins is summed, both for the $r_t'_{up}$ and $r_t'_{low}$ circles. Then, equations analgous to Eqs. (52) and (53) are used to determine the weighted difference due to the $r_t'_{up}$ and $r_t'_{low}$ contributions.

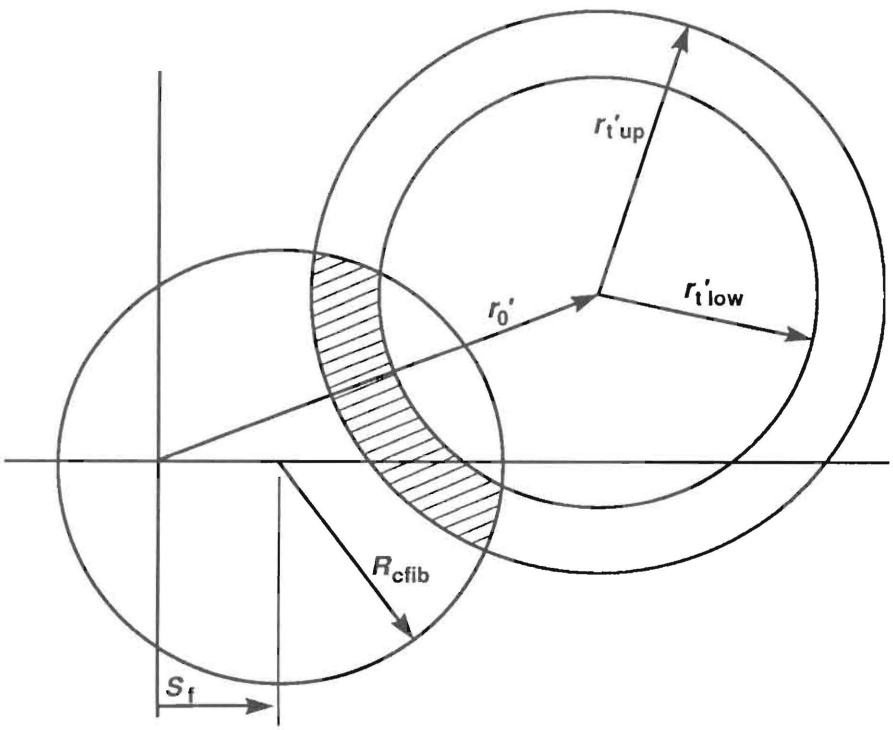

Figure 15. The illumination at the fiber plane due to light from a specific small area on the reflector and due to a particular r_t' bin. The light in the shaded area can enter the off-axis fiber.

The result of the above is a quantity called power and represents the collected light due to just one r_t' bin. A macro drives the POWERX spreadsheet, varying the r_t' bin boundaries, and putting the 10 values of power into a table called "powertable." Powertable is then summed to give the collected light for a given reflector travel. Figure A-3 shows the input-output part of POWERX, which takes about ten minutes to calculate nine reflector travel positions. Revised versions run in 4 minutes. Figure 16 shows our standard problem estimated by POWERX. The agreement with the Monte Carlo results of McMillan is better.

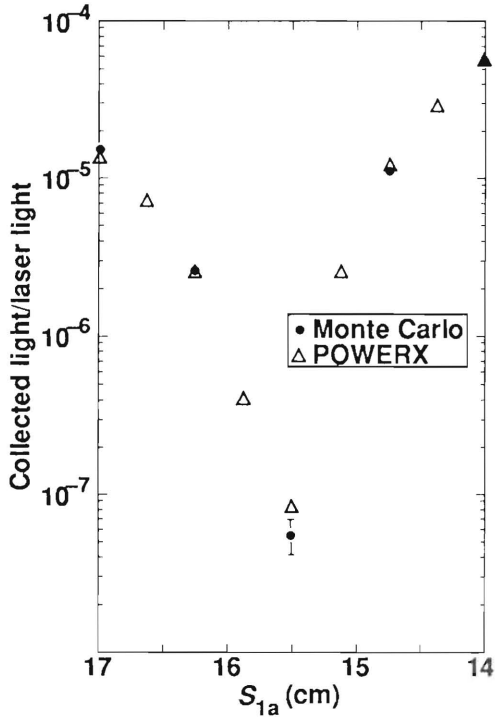

Figure 16. The collected light vs reflector travel position as estimated by POWERX and Monte Carlo.

POWERX8—the Most Accurate Code

Finally, POWERX8 was written to improve upon POWERX in two ways. First, the accuracy was to be increased by (1) doing the summations in finer steps and (2) providing to the user a printout of illumination at the fiber plane vs radius. POWERX will not do the latter. Second, POWERX8 is written using a formalism different from POWERX so that the two codes can be used to verify in some sense the accuracy of the other, with a minimum of common sources of error.

POWERX8 calculates the power distribution on the fiber plane over the region where the collection fiber resides, and then integrates it over the off axis fiber. Figure 17 shows the boundary of the collection fiber, which may be on- or off-axis. Since the laser fiber and the lens are centered on the axis, the illumination at the fiber plane depends only upon the radius r'. POWERX8 chooses 20 values of r' from

$$r'_{\min} = \max(0, S_f - Rcfib) \tag{54}$$

to

$$r'_{\max} = \min(S_f + R_{cfib}, r_t'_{\max} + r_{t\max}/mag + R_{lfib}) \ . \tag{55}$$

The second term in Eq. (55) is there because no illumination exists at the fiber plane for r' greater than this value. Thus the r' values are

$$r' = r'_{\min} + dr' \cdot (j - 0.5) \ , \tag{56}$$

where j varies from 1 to 20, and

$$dr' = (r'_{\max} - r'_{\min})/20 \ . \tag{57}$$

The length of the circular arc at radius r_j' is

$$L(r_j') = 2 \cdot r_j' \cdot \cos^{-1}\left(\frac{S_f^2 + r_j'^2 - R_{cfib}^2}{2 \cdot r_j' \cdot S_f}\right) , \tag{58}$$

if $|S_f - R_{cfib}| \le r_j'$; otherwise,

$L(r_j') = 2\pi \cdot r_j'$ if $R_{cfib} > S_f$; otherwise,

$L(r_j') = 0$.

The collected power is the sum over the 20 bins of the product of the power per unit area, $dI(r_j')/dA$ times the length $L(r_j')$ times dr'.

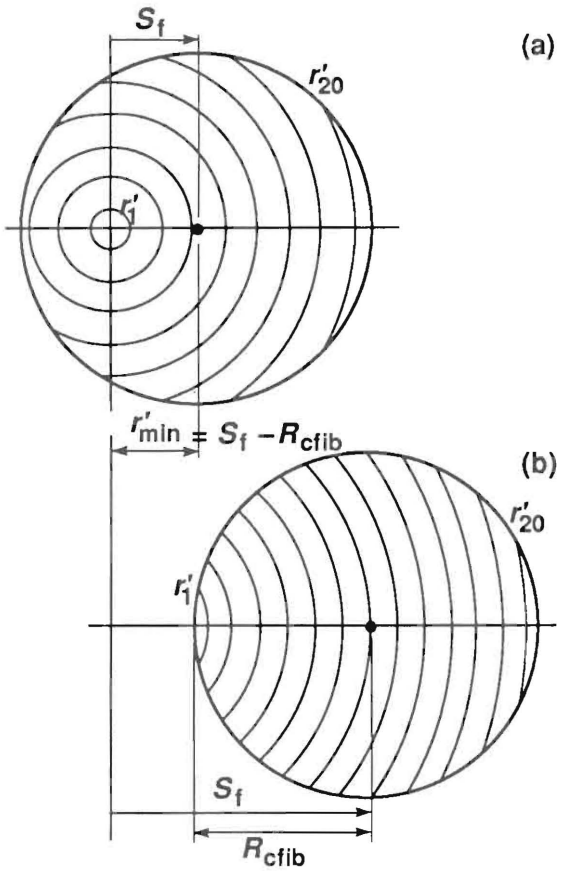

Figure 17. (a) Arcs of constant intensity at the fiber plane that intercept the off-axis collection fiber of radius R_{cfib} and offset S_f, such that the axis is within the fiber. (b) The case where the axis is outside the fiber.

To evaluate dI/dA on the fiber plane at a specific radius r_j', note from Fig. 18(a) that the minimum radius at the reflector, r_{jmin}, that can contribute is

$$r_{jmin} = \max[0, mag \cdot (r_j' - r_t'_{max})] \ . \qquad (59)$$

This is because light reflected from radius $rjmin$ emitted into the largest-diameter r_t' bin just reaches the radius r_j' at the fiber plane. Also, the maximum radius at the reflector, r_{jmax}, that can contribute is

$$r_{jmax} = \min[mag \cdot (r_j' + r_t'_{max}), \quad mag \cdot R_{lfib} + r_{tmax}] \ . \qquad (60)$$

Here, the first term arises from Fig. 18(b), and the second from the limited extent of illumination at the reflector.

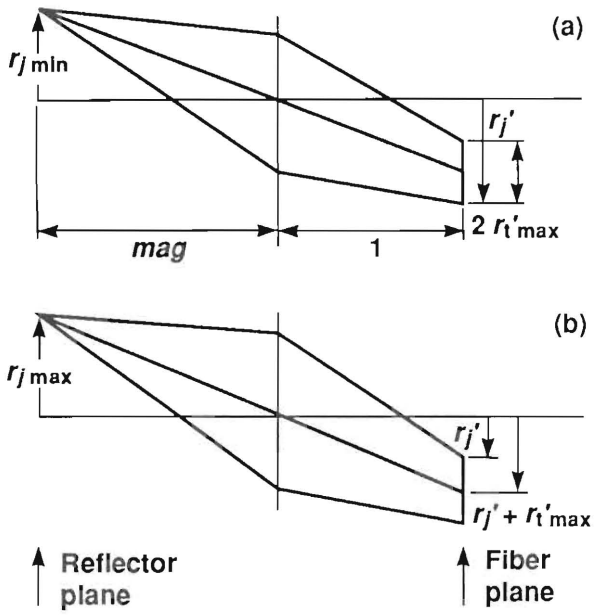

Figure 18. Illustration of the origins of Eqs. (59) and (60). (a) R_{jmin} is the smallest radius at the reflector that makes an illumination at the fiber plane that can include the particular radius r_j'. (b) R_{jmax} is the maximum radius making illumination at r_j'.

Thus, for each r_j' on the fiber plane, POWERX8 choses 20 values of r_{ji} on the reflector defined by

$$r_{ji} = r_{jmin} + dr_j \cdot (i - 0.5) \ , \text{for } 1 \le i \le 20 \ . \qquad (61)$$

and where

$$dr_j = (r_{jmax} - r_{jmin})/20 \ . \qquad (62)$$

These radial bins at the reflector are as in Fig. 19.

We need to evaluate $dI(r_{ji})/dA$, on the reflector at radius r_{ji}, as well as the overlap area at the fiber plane for each i, given a particular r_t' bin. For now, we fix S_{1a}, the r_t and r_t' bins, and the 20 r_j' values. Consider one annular source of reflected light from the bin whose average radius is r_{ji}, as shown in Fig. 20(a). Light leaving a very small shaded area $r_{ji} \cdot dr_j \cdot d\phi = dA$ from one r_t' bin makes on the fiber plane an illumination of intensity

$$\text{Illum} = \frac{I(r_{ji}) \cdot dA \cdot F\Omega}{\pi \cdot (r_t'^2_{up} - r_t'^2_{low})} \ . \qquad (63)$$

over an annulus shown in Fig. 20(b).

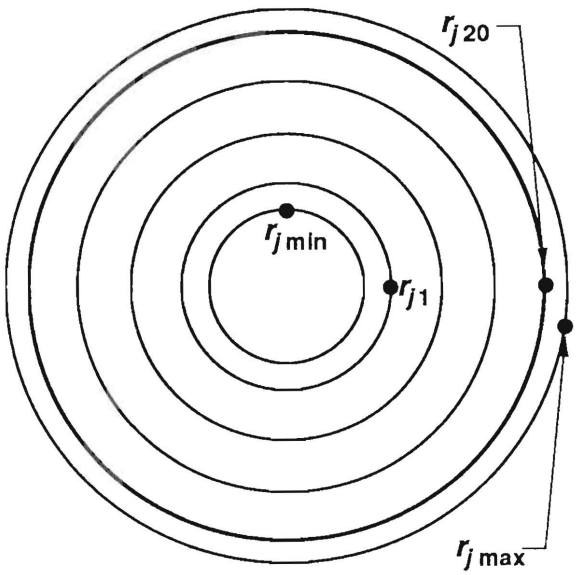

Figure 19. Locations of the radii r_{ji} at the reflector for a given j value.

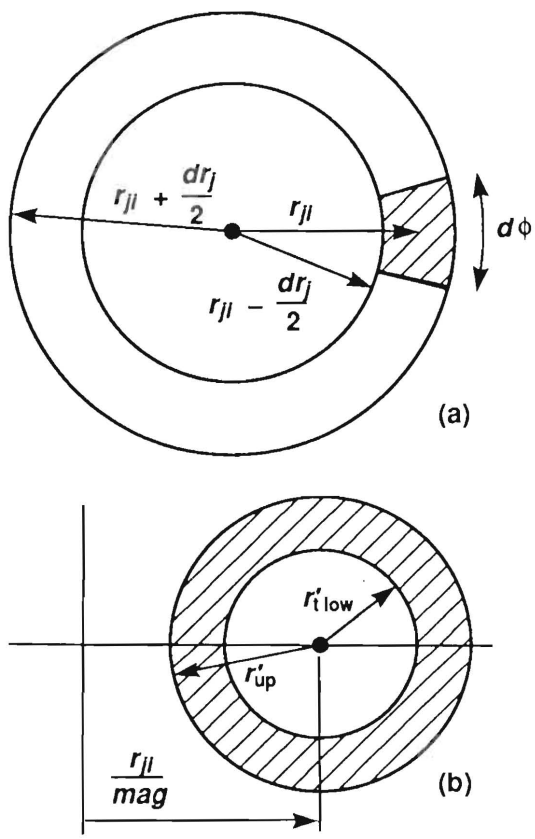

Figure 20. (a) A small shaded area at the reflector. (b) The illumination at the fiber plane made by the shaded area.

Given r_j' on the fiber plane, we must determine what fraction of the r_{ji} annulus above makes an annular pattern due to one r_t' bin that illuminates one specific r_j' point. The entire r_{ji} annulus of Fig. 20(a) makes a collection of illumination centers on the fiber plane, which is the demagnified annulus shown in Fig. 21. Here, we have

$$r_0'{}_{low} = \frac{r_{ji} - dr_j/2}{mag} = \frac{r_{j\,min} + dr_j \cdot (i-1)}{mag} \tag{64}$$

and

$$r_0'{}_{up} = r_0'{}_{low} + dr_j/mag \ . \tag{65}$$

Both $r_0'{}_{low}$ and $r_0'{}_{up}$ depend on j and i.

Still considering only one r_t' bin and one r_{ji} annulus, the point r_j' on the fiber plane is illuminated by all points within the r_{ji} annulus whose corresponding illumination centers in the r_0' annulus of Fig. 21 lie a distance from r_j' between $r_t'{}_{lower}$ and $r_t'{}_{upper}$. This is illustrated in Fig. 22, where all illumination centers within the shaded area can illuminate point A at radius r_j'.

Figure 20(a) showed that an area dA on the reflector made an illumination power per unit area on the fiber plane equal to Illum of Eq. (63). The number of contributing areas on the reflector of area dA that correspond to the shaded area in Fig. 22 is equal to that shaded area divided by dA multiplied by the magnification squared. Each r_t' bin at the fiber plane has a certain weight, which is defined as the fraction of all the rays traced through the lens which end up in that bin. Now we can state that the power per unit area at radius r_j' due to only one r_t' bin of weight $w(r_t')$ and to only one r_{ji} annulus at the reflector is

$$\frac{dI(r_j', r_t', r_{ji})}{dA} = \frac{I(r_{ji}) \cdot F\Omega \cdot \text{weight}(r_t') \cdot (\text{Fig. 22 shaded area})}{\pi \cdot (r_t'{}_{up}^2 - r_t'{}_{low}^2)} \ . \tag{66}$$

The shaded area of Fig. 22 is determined by four applications of the results of Eqs. (36) through (39) and Fig. 4. The quantity r there is replaced by r_j' now; r_t is replaced by either $r_t'{}_{up}$ or $r_t'{}_{low}$; and r_0 is replaced by either $r_0'{}_{up}$ or $r_0'{}_{low}$. The two overlap areas calculated by using $r_0'{}_{up}$ with $r_t'{}_{low}$ and $r_0'{}_{low}$ with $r_t'{}_{up}$ both

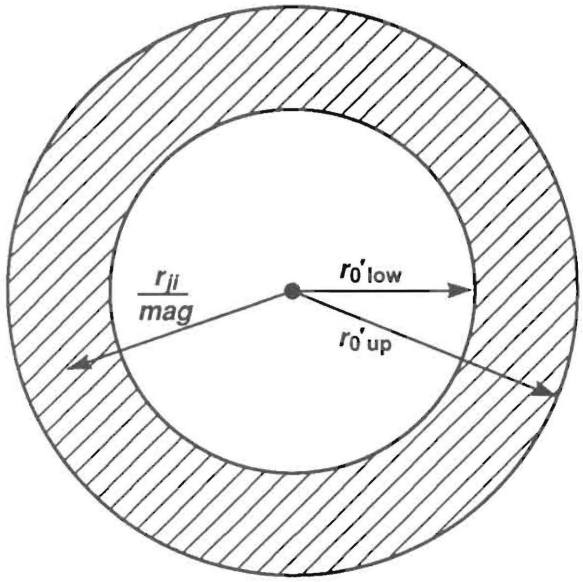

Figure 21. The locus of all illumination centers at the fiber plane made by the r_{ji} annulus of Fig. 20(a).

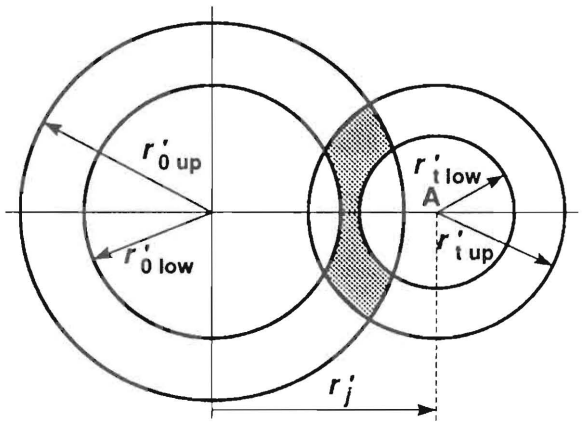

Figure 22. The shaded area is the locus of all illumination centers that can illuminate the r_j' point labeled A.

subtract from the two areas determined by using $r_0'_{up}$ with $r_t'_{up}$ and $r_0'_{low}$ with $r_t'_{low}$ to determine the overlap area of Fig. 22. The latter can have many shapes different from that of Fig. 22, but the net overlap is still calculated the same way. This is easily confirmed by drawing pictures of all the shaded area shapes that can occur for Fig. 22 when varying the thicknesses of the annuli and the spacing between their centers.

The resulting $dI(r_j')/dA$ is then multiplied by $L(r_j') \cdot dr'$ [see Eq. (58)] and then summed over j to give the total light entering the collection fiber within its numerical aperture.

POWERX8 takes over two hours to run, and the result is shown in Figs. 23 and A-4 compared with McMillan's Monte Carlo results. The agreement is the same as with POWERX. POWERX8 calculates the power distribution on the reflector in 30 radial bins and uses macros heavily. The latter increases computing time, but otherwise the code is too large for many PC memories.

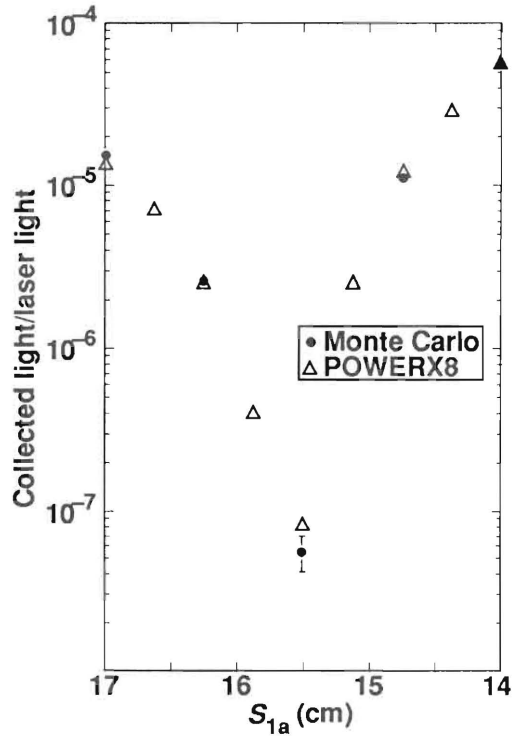

Figure 23. POWERX8 results vs McMillan's Monte Carlo calculation.

Summary

The agreement of POWERX8 with the Monte Carlo result confirms our assumption that coma is negligible. The near agreement between POWERX and POWERX8 is satisfying because the mathematical approach to the two codes is quite different. POWERX8 was expected to be more accurate than POWERX because of its finer binning. In practice, however, POWERE or POWERX is probably the most useful for initial approximate calculations for a new configuration at reasonable computation time. POWERX8 presently is best suited for use on a PC for overnight runs, with parameters inferred from previous POWERE or POWERX runs. Recently available programs for Symphony spreadsheets that allow them to run them in a compiled mode may decrease computation time significantly.

References

1. C. F. McMillan, D. R. Goosman, N. L. Parker, L. L. Steinmetz, H. H. Chau, T. Huen , R. K. Whipkey, and S. J. Perry, *Rev. Sci. Instrum.* **59**, 1 (1988).
2. C. F. McMillan, N. L. Parker, and D. R. Goosman, *Appl. Opt.* **28**, 826 (1989).
3. D. R. Goosman, Lawrence Livermore National Laboratory, Livermore, Calif., UCRL-100589 Rev 1 (1989) (to be published in *Appl. Opt.*).
4. C. F. McMillan, Lawrence Livermore National Laboratory, Livermore, Calif., private communication (1990).

Appendix: Format of the POWER Code

User inputs are listed in natural order from the fiber end through the lens to the reflector (in mm). Figure A-1 is a sample output from the code.

R_{lfib}	Radius of laser fiber.
NA_l	Numerical aperture of laser fiber.
R_{cfib}	Radius of collection fiber.
NA_c	Numerical aperture of collection fiber.
S_f	Distance from collection fiber center to axis—may be zero.
r_3'	Radius of curvature of rightmost lens surface—positive for Fig. 2.
n_2'	Index of refraction of right part of lens.
T_2'	Separation on axis between rightmost two lens surfaces.
r_2'	Radius of curvature of mid-lens surface—positive for Fig. 2.
n	Index of refraction of left part of lens.
T	Separation on axis between leftmost two lens surfaces.
r_1'	Radius of curvature of leftmost lens surface—positive for Fig. 2.
L_{1f}	Distance from fibers to midway between leftmost two lens surfaces.
Rad_{1a}	Maximum radius of aperture at the lens.
F_{1a}	Paraxial focal length of lens—for reference only; not used.
λ	Wavelength of light used for diffraction contribution to blur.
H_{left}	x coordinate of the left principal point of lens.
H_{right}	x coordinate of the right principal point of lens.

(For biconvex lenses ($n_2' = 1$), formulae for H_{left}, H_{right}, and F_{1a} may be substituted for user input numbers.)

Start	Distance along the axis from reflector to midway between the leftmost two surfaces of the lens at start of reflector travel.
Travel	Travel distance—the macro "s" varies S_{1a} (Fig. 3) from "start" to (start-travel) in equally spaced steps.
Blurs	Enter "yes" if maximum blurs are wanted; any other entry produces a calculation for weighted blurs.

The following quantities are calculated by the code (listed as a function of reflector position S_{1a}:

R_{lower}	Radius out to which reflector illumination is uniform.
R_{upper}	Radius out to which reflector illumination is nonzero.
R_{half}	Average of R_{lower} and R_{upper}.
Power	Watts entering collection fiber within its numerical aperture per watt emitted by the laser fiber (lossless Lambertian reflector).
r_t	Radius of illumination on reflector as a result of a point source from the laser fiber.
r_t'	Radius of illumination at fiber plane due to a point source from the reflector.
r_0	$r_{1fib} \cdot (S_{1a} + H_{left})/(L_{1f} - H_{right})$.

At the right in Figure A-1 are single values of the following quantities:

x_e	Center of curvature of leftmost lens surface = $T/2 - r_2'$.
x_f	Center of curvature of mid lens surface = $-T/2 + r_1'$.
x_g	Center of curvature of rightmost lens surface = $T/2 + T_2' - r_3'$.
x_h	x coordinate of point $h = [(r_1')^2 - (r_2')^2 - (x_f)^2 + (x_e)^2]/[2 \cdot (x_e - x_f)]$.
y_h	y coordinate of point $h = \sqrt{[(r1')^2 - (x_h - x_f)^2]}$.
Ratio	Ratio of maximum to minimum of the collected power table.
L_{Size}	Radius of laser illumination at the right end of the lens if no aperture were present $= (L_{1f} - T/2 - T_2') \cdot \tan[\sin^{-1}(NA_1)]$.
R_{ill}	Illumination radius at lens = $\mathrm{Min}(Rad_{1a}, L_{Size})$.
Powf	Fraction of laser power that hits the lens with aperture $Rad_{1a} = \mathrm{Min}[1, (Rad_{1a}/L_{Size})^2]$.
S_{1af}	Paraxial conjugate to $L_{1f} = [F_{1a}^{-1} - (L_{1f} - H_{right})^{-1}]^{-1} - H_{left}$ (printed only for reference, not used in code).
TEST	Equals unity if T is large enough for desired Rad_{1a} value.
T_{min}	Minimum value of $T = A - B - \sqrt{[(A - B)^2 - 2 \cdot A \cdot (r_1' - B)]}$, where $A = r_1' + r_2'$ and $B = \sqrt{[(r_1')^2 - Rad_{1a}^2]}$.
mag	Magnification from fiber to reflector = $(S_{1a} + H_{left})/(L_{1f} - H_{right})$.
RefRad	Radius of reflected illumination used. Ensures that rays entering collection fiber are within its numerical aperture, which is the smaller of (Rad_{1a}) or $(L_{1f} - T/2 - T_2') \cdot \tan[\sin^{-1}(NA_c)]$.
F	Solid angle factor for lens = $(RefRad/S_{1a})^2$ = fraction of Lambertian that is intercepted by aperture of radius *RefRad*.

This code takes 25 s to calculate the power at nine reflector positions when run on an IBM XT with an Intel Inboard PC 80386 processor.

```
Power - 5/17/90- 2 element lens- see page 1a2 of 12/22/89 notes
          Enter yes if you want maximum blurs (off axis fiber)
          Ten phi and ten radial bins
          Origin is T/2 mm to the right of left (reflector) edge of lens
 Rlfib    NAl    Rcfib   NAc      Sf       r3'     n2'    T2'     r2'     n      T
  0.05     0.1    0.05   0.22     0.125  136.95   1.649      1  10.908  1.517      4
       Takes 25 seconds to calc                          S1a           Maximum
  r1'     L1f    Rad1a   F1a    lambda    Hleft  Hright  Start  Travel  Blurs?
10.948    28.3       4  24.59         0   -1.45  -0.413    170      30  yes

  S1a   Rlower  Rupper  Rhalf    Power     rt      rt'     ro     xe      xf     xg
 170.0   0.054   0.533  0.294  2.35E-05   0.239   0.084  0.293  -8.908  8.948  -133.
 166.3   0.117   0.457  0.287  1.55E-05   0.170   0.069  0.286    xh      yh   Ratio
 162.5   0.180   0.381  0.280  7.17E-06   0.100   0.054  0.280  -0.004  6.302    274
 158.8   0.225   0.323  0.274  1.30E-06   0.049   0.038  0.273  LSize    Rill   PowF
 155.0   0.181   0.354  0.267  1.20E-07   0.087   0.021  0.267  2.5427   2.54      1
 151.3   0.128   0.394  0.261  1.33E-06   0.133   0.025  0.260   S1af    TEST   Tmin
 147.5   0.068   0.441  0.254  6.79E-06   0.187   0.037  0.254   172.6      1   1.52
 143.8   0.000   0.495  0.248  1.75E-05   0.248   0.049  0.247    Mag   RefRad   F
 140.0   0.075   0.558  0.316  3.29E-05   0.316   0.064  0.241    4.83      4  8E-04
```

Figure A-1. Sample output from the POWER code. The reflector travels from 170 to 140 mm from the origin of coordinates. Input quantities are displayed in the upper two numeric lines. The lower nine lines are results. Definitions are found on pages 18 and 19. The spot radius at the reflector, R_{half}, stays below 0.32 mm, and the collected power dips near S_{1a} = 155 mm. See also Fig. 12.

```
Powere  - 10/30/90- rebin rt' fan angles for better weighting
      Ten r and ten phi bins, and ten blur bins
      Dont set Sf=0
      Uses ray-tracing determined reflector intensity distribution
Rlfib    NAl    Rcfib   NAc      Sf       r3'     n2'    T2'     r2'     n      T
 0.05     0.1    0.05   0.22     0.125  136.94   1.649      1  10.91  1.517      4
      Input matches McM's 4/2/90 calculation          S1a           Maximum
 r1'     L1f    Rad1a   F1a    lambda    Hleft  Hright  Start  Travel Blurs?  FRavg
10.95    28.3       4  24.59         0   -1.45  -0.413    170      30  yes     0.006

 S1a   R(Imax)R(I=0)   Rhalf    Power    rtmax    rt'     ro     xe      xf     xg
170.0   0.000   0.533  0.280  1.78E-05   0.239   0.075  0.293  -8.90  8.948  -133.9
166.3   0.000   0.457  0.280  1.02E-05   0.170   0.061  0.286    xh      yh   Ratio
162.5   0.000   0.381  0.279  3.60E-06   0.100   0.046  0.280  -0.00  6.302  894.99
158.8   0.000   0.323  0.273  3.51E-07   0.049   0.031  0.273  LSize    Rill   PowF
155.0   0.000   0.354  0.260  4.32E-08   0.087   0.016  0.267  2.542   2.54      1
151.3   0.000   0.394  0.239  2.32E-06   0.133   0.025  0.260   S1af    TEST   Tmin
147.5   0.000   0.441  0.206  9.97E-06   0.187   0.036  0.254  172.6      1   1.52
143.8   0.000   0.495  0.155  2.29E-05   0.248   0.049  0.247    Mag   RefRad   F
140.0   0.127   0.558  0.360  3.86E-05   0.316   0.064  0.241    4.83      4  0.0008
```

Figure A-2. Input and partial output from POWERE. The R_{half} values here are more accurate than those in POWER because of radial binning in POWERE. See also Fig. 14.

```
Powerx - 3/8/91

      Invoke macro called "s" to start

Rlfib   NAl   Rcfib   NAc     Sf      r3'    n2'   T2'   r2'    n      T
 0.05    0.1   0.05   0.22    0.125 136.95  1.649     1 10.91 1.517      4
                                                   S1a
 r1'    L1f   Rad1a   F1a   lambda   Hleft Hright Start Travel
10.95   28.3      4  24.59        0  -1.45 -0.413   170    30

 S1a  R(Imax)R(I=0)  Rhalf   Power   rtmax rt'max   ro    xe    xf    xg
170.0  0.000  0.533  0.280 1.37E-05  0.239  0.084 0.293 -8.91 8.948 -133.9
166.3  0.000  0.457  0.284 7.45E-06  0.170  0.069 0.286   xh    yh  Ratio
162.5  0.000  0.381  0.279 2.70E-06  0.100  0.054 0.280 -0.00 6.302 532.01
158.8  0.000  0.323  0.273 4.25E-07  0.049  0.038 0.273 LSize  Rill  PowF
155.0  0.000  0.354  0.263 8.63E-08  0.087  0.021 0.267 2.542  2.54      1
151.3  0.000  0.394  0.240 2.38E-06  0.133  0.025 0.260  S1af  TEST  Tmin
147.5  0.000  0.441  0.206 1.21E-05  0.187  0.037 0.254 172.6     1   1.52
143.8  0.000  0.495  0.156 2.82E-05  0.248  0.049 0.247  Mag  RefRad   F
140.0  0.093  0.558  0.357 4.59E-05  0.316  0.064 0.241  4.83     4 0.0008
```

Figure A-3. Input and partial output from POWERX. See also Fig. 16.

```
Powerx8 - 5/18/90- rebin rt' fan angles for better weighting-but rt binning
         Setting Sf=0 masks out radius=Rill for return light
         and modifies F- also calculates radial dist on fiber
      20 radial, phi, rt, and rt' bins with macros
Rlfib   NAl   Rcfib  NAc     Sf      r3'    n2'   T2'   r2'    n      T
 0.05    0.1   0.05  0.22    0.125 136.95  1.649     1 10.908 1.517      4
Still could ray trace to better define Refrad    S1a
 r1'    L1f   Rad1a  F1a   lambda   Hleft Hright Start Travel        FRavg
10.95   28.3      4 24.59        0  -1.45 -0.413   170     30        0.008
takes 15 minutes per S1a value-
 S1a  R(Imax)R(I=0) Rhalf   Power   rtmax rt'max   ro    xe    xf    xg
170.0  0.000  0.533 0.283 1.37E-05  0.239  0.084 0.293 -8.908 8.948 -133.9
166.3  0.004  0.457 0.287 7.37E-06  0.170  0.069 0.286   xh    yh  Ratio
162.5  0.013  0.381 0.279 2.64E-06  0.100  0.054 0.280 -0.004 6.302 548.12
158.8  0.021  0.323 0.273 4.00E-07  0.049  0.038 0.273 LSize  Rill  PowF
155.0  0.029  0.354 0.259 8.40E-08  0.087  0.021 0.267 2.5427  2.54      1
151.3  0.026  0.394 0.237 2.40E-06  0.133  0.025 0.260  S1af  TEST  Tmin
147.5  0.020  0.441 0.205 1.21E-05  0.187  0.037 0.254  172.6     1   1.52
143.8  0.014  0.496 0.219 2.83E-05  0.248  0.049 0.247   Mag  RefRad   F
140.0  0.100  0.558 0.358 4.61E-05  0.316  0.064 0.241   4.83     4  8E-04
```

Figure A-4. Input and partial output from POWERX8. See also Fig. 23.